Applied Catalysis A: General 405 (2011) 69–78

Contents lists available at ScienceDirect

Applied Catalysis A: General

journal homepage: www.elsevier.com/locate/apcata

Influence of the thermal treatment on the physicochemical properties and photocatalytic degradation of 4-chlorophenol in aqueous solutions with tungstophosphoric acid-modified mesoporous titania

Mirta Blanco, Luis Pizzio*

Centro de Investigación y Desarrollo en Ciencias Aplicadas "Dr. J. J. Ronco" (CINDECA), Departamento de Química, Facultad de Ciencias Exactas, UNLP-CCT La Plata, CONICET, 47 No. 257, 1900-La Plata, Argentina

ARTICLE INFO

Article history:
Received 25 April 2011
Received in revised form 14 July 2011
Accepted 22 July 2011
Available online 30 July 2011

Keywords:
Mesoporous titania
Tungstophosphoric acid
4-Chlorophenol
Photocatalytic degradation

ABSTRACT

Materials based on titania directly modified with tungstophosphoric acid were prepared using titanium isopropoxide as titania precursor and urea as a low-cost pore-forming agent. The obtained mesoporous solids presented an average pore diameter higher than 3.1 nm. The specific surface area decreased when the TPA amount and the calcination temperature increased. All the modified solids only showed the anatase structure of titania by X-ray diffraction, while for the unmodified sample this structure was transformed into the rutile phase from 600 °C on. The crystallite size increased with the calcination temperature, though the TPA-modified samples presented lower values when the TPA amount was increased. The ^{31}P nuclear magnetic resonance studies showed that the Keggin structure of the tungstophosphate anion was partially transformed when it was thermally treated up to 600 °C, though structure disruption took place at higher temperature. The band gap values estimated from the UV–vis-diffuse reflectance spectra did not show important variation, though they slightly decreased with the TPA content. The 4-chlorophenol degradation was studied in liquid phase, with an air flow continuously bubbled. The degradation behavior of the catalysts as a function of time depended on the TPA amount and the thermal treatment temperature, the samples containing 30% TPA calcined at 500–600 °C and 20% TPA calcined at 600 °C being more effective. The apparent reaction constant, estimated assuming a pseudo-first-order kinetics, followed the same trend. The catalysts can be reused at least three times without an important decrease in the degradation and mineralization degrees.

1. Introduction

Chlorinated phenols constitute an important class of water and air contaminants due to their high toxicity to living organisms, bioaccumulation, strong odor emission and persistence in the environment. They are widely used in the industry and cause severe environmental problems, because they are carcinogens and mutagens. Among them, 4-chlorophenol (4-CP), a known toxic and nonbiodegradable organic compound, is present in the wastewater of pulp and paper, dyestuff, pharmaceutical and agrochemical industries [1].

4-CP is currently removed from the wastewater by conventional treatment methods such as chlorination, adsorption, and biological treatment. However, each method has its shortcomings. For example, chlorination treatments often generate carcinogenic by-products, the spent activated carbon employed in commercial adsorption processes needs to be safely disposed [2] and the biological process usually requires a considerably long treatment period to reduce 4-CP to an acceptable level in the final effluent [3].

Photolytic oxidation processes using semiconductor materials have been accepted as a promising alternative to the conventional methods because most of the pollutants can be completely mineralized to CO_2 with suitable catalysts in the presence of UV light. Among the semiconductors employed, TiO_2 is considered to be a good photocatalyst due to its high capacity for degrading toxic and recalcitrant chemical species via relatively simple and low-cost procedures, nontoxicity, easy availability, and long-term stability [4–7].

The photocatalytic degradation of 4-CP has been investigated by many research groups and has become a standard reaction for evaluating various experimental parameters in photocatalysis [8].

Titania performance in the photodegradation of contaminants contained in wastes is influenced by the crystal structure, the crystallinity, the surface area, the porosity, the surface hydroxyl density, and the band gap energy [8–11], among other factors.

The low surface area and the fast recombination of the photoinduced electrons and holes are the main effects that can lead to a low photocatalytic activity. So, an increase in the surface area and

* Corresponding author. Fax: +54 221 425 4477.
E-mail address: lrpizzio@quimica.unlp.edu.ar (L. Pizzio).

0926-860X/$ – see front matter © 2011 Elsevier B.V. All rights reserved.
doi:10.1016/j.apcata.2011.07.030

the separation of electrons and holes can improve the photocatalytic activity of titania. Sol–gel reactions using urea as a low-cost pore-forming agent were found to be a good method to synthesize mesoporous titania with suitable properties to be used as a photocatalyst [12,13].

Transition metals or metal oxides were proved to be electron trappers, thus avoiding the recombination of the electron–hole pairs of TiO_2-based catalysts [14–17] and improving the photocatalytic activity. In addition, it has been reported that the light absorption is extended to the visible region when large band gap semiconductors are doped with suitable transition metal ions [18].

The increment of the photoactivity of titania samples modified with W has been mainly explained by considering the formation of intermediate W(V) species by means of a transfer of photogenerated electrons [19,20]. This reduced W species could be oxidized to W(VI) by transferring electrons to oxygen [21].

Indeed, several transition metal ions lead to a band gap shift to the visible region when they are impregnated on large band gap semiconductors, allowing the use of light from the visible region of the spectrum.

Heteropolyoxometallates (POM) are widely used as oxidation as well as acid catalysts [22–24]. They are also employed as effective homogeneous photocatalysts in the degradation of organic pollutants in water [25–27].

POM absorb strongly in the near visible and UV region of the light spectrum ($\lambda < 400$ nm). This absorption corresponds to the ligand-to-metal charge-transfer band and it can generate strongly oxidizing excited state POM* (reaction (1)). They are able to carry out the oxidation of organic substrates (S) (reaction (2)) directly via charge transfer or H-atom abstraction, or indirectly through the intermediacy of solvent-derived radicals [27]. After that, the corresponding reduced POM are usually reoxidized to their original oxidation state by an electron acceptor such as dioxygen (reaction (3)).

$$POM + h\nu \rightarrow POM^* \quad (1)$$

$$POM^* + S \rightarrow POM^- + S^+ \quad (2)$$

$$POM^- + O_2 \rightarrow POM + O_2^- \quad (3)$$

POM have been added to TiO_2 suspensions [28], incorporated into TiO_2 colloids [29], or anchored to TiO_2 by chemical interactions [30] with the purpose of reducing the charge recombination in UV-illuminated TiO_2. The capacity of POM as acceptors (reaction (5)) of the electrons, generated in the conduction band (e_{cb}^-) together with holes in the valence band (h_{vb}^+), of UV-irradiated TiO_2 suspensions (reaction (4)) was demonstrated by Park and Choi [31] using a photoelectrochemical method. The reduced POM react with O_2 to generate superoxides (reaction (3)).

$$TiO_2 + h\nu \rightarrow e_{cb}^- + h_{vb}^+ \quad (4)$$

$$POM + e_{cb}^- \rightarrow POM^- \quad (5)$$

Unlike these researchers, who have modified the surface of previously prepared TiO_2 with POMs [28–31], we studied the incorporation of tungstosilicic and tungstophosphoric acid into the titania matrix during the TiO_2 gel synthesis, in a similar way to Li et al. [32], but using urea as low-cost template with the purpose of obtaining mesoporous materials [33,34]. We also studied the catalytic activity in the methyl orange photodegradation of the solids annealed in the temperature range 100–600 °C and correlated it with their physicochemical properties [35,36].

As a continuation of this previous work, in the present paper we have extended the temperature range of treatment in order to explore the effect on the crystal structure, textural and physicochemical properties of the tungstophosphoric acid (TPA)/mesoporous titania composites synthesized via HCl catalyzed sol–gel reactions, where urea is used as a low-cost pore-forming agent.

The aim of our research is to correlate the catalytic activity in the 4-chlorophenol photodegradation with the structural and textural characteristics of the solids, and to discuss the effect of the preparation variables on the pollutant degradation.

2. Experimental

2.1. Synthesis of TPA-modified mesoporous titania

A titanium isopropoxide (Aldrich, 26.7 g) solution was prepared in absolute ethanol (Merck, 186.6 g) under N_2 atmosphere and at room temperature, continuously stirring for 10 min. Then, 0.33 cm^3 of a 0.28 M HCl aqueous solution was slowly added in order to catalyze the sol–gel reaction. After 3 h, 120 g of a urea–ethanol–water (1:5:1 weight ratio) solution was added, together with an ethanol solution of tungstophosphoric acid ($H_3PW_{12}O_{40}{\cdot}23H_2O$, Fluka p.a.) under vigorous stirring. The amount of TPA was varied with the purpose of obtaining a TPA concentration of 0%, 10%, 20% and 30% by weight in the final solid (named TiTPA00, TiTPA10, TiTPA20, and TiTPA30, respectively). The gels were dried at room temperature, and the solids were ground into powder and extracted with distilled water for three periods of 24 h, in order to remove the urea.

Finally, the solids were thermally treated at 100, 500, 600, 700 and 800 °C for 2 h ($TiTPAXX_{T100}$, $TiTPAXX_{T500}$, $TiTPAXX_{T600}$, $TiTPAXX_{T700}$, and $TiTPAXX_{T800}$, respectively, where XX is the TPA concentration).

2.2. Sample characterization

The specific surface area, the pore volume and the mean pore diameter of the solids were determined from the N_2 adsorption–desorption isotherms at the liquid-nitrogen temperature, obtained using Micromeritics ASAP 2020 equipment. The solids were previously degassed at 100 °C for 2 h.

The X-ray diffraction (XRD) patterns were recorded with Philips PW-1732 equipment with a built-in recorder, using Cu Kα radiation, nickel filter, 20 mA and 40 kV in the high voltage source, and scanning angle between 5 and 60° 2θ at a scanning rate of 1° per minute.

The solids were studied by transmission electron microscopy (TEM) in a JEOL 100 CXII microscope, working at 100 kV and at a magnification of 80,000×. The samples were crushed in an agate mortar, ultrasonically dispersed in isobutanol, and deposited on a carbon-coated copper grid. The particle size distribution of the samples was determined by manual image analysis of a few hundred particles.

The secondary electron micrographs of the samples were obtained by scanning electron microscopy (SEM), using Philips Model 505 equipment.

The ^{31}P magic angle spinning-nuclear magnetic resonance (^{31}P MAS-NMR) spectra were recorded with Bruker Avance II equipment, using the CP/MAS ^1H–^{31}P technique. A sample holder of 4 mm diameter and 10 mm in height was employed, using 5 μs pulses, a repetition time of 4 s, and working at a frequency of 121.496 MHz for ^{31}P at room temperature. The spin rate was 8 kHz and several hundred pulse responses were collected. Phosphoric acid 85% was employed as external reference.

The Fourier transform infrared (FT-IR) spectra of the solids were obtained using a Bruker IFS 66 FT-IR spectrometer and pellets in KBr in the 400–4000 cm^{-1} wavenumber range.

The diffuse reflectance spectra (DRS) of the materials were recorded using a UV-visible Lambda 35, Perkin Elmer spectrophotometer, to which a diffuse reflectance chamber Labsphere

RSA-PE-20 with an integrating sphere of 50 mm diameter and internal Spectralon coating is attached, in the 200–800 nm wavelength range.

2.3. Photodegradation reaction

The catalytic activity of the materials was evaluated in the photodegradation of 4-chlorophenol (Fluka) in water, at 25 °C. The tests were carried out employing a 125 W high-pressure mercury lamp (with a maximum emission at about 365 nm) placed inside a Pyrex glass jacket, thermostated by water circulation, and immersed in the 4-chlorophenol (4-CP) solution contained in a 300 ml cylindrical Pyrex glass reactor. The catalyst is maintained in suspension by stirring, and air is continuously bubbled. Previously, the 4-CP solution (200 ml, 1.5×10^{-4} mol/l) containing 100 mg of catalyst was magnetically stirred in the absence of light for 60 min to ensure that the adsorption–desorption equilibrium of 4-CP on the surface of the materials is attained. During the course of the experiments, samples (3 ml) were periodically withdrawn, filtered using a Millipore syringe adapter (porosity, 0.45 μm) and then analyzed. The variation of the 4-CP concentration as a function of the reaction time was determined by a UV-visible LAMBDA 35 Perkin Elmer double-beam spectrophotometer, measuring the absorbance at 225 nm. The concentration of released chloride ions was measured by a selective Cl^- electrode (pHoenix CLO1508) with an ion meter (Consort P903). The filtrates were extracted three times with ethyl ether, the organic layers were collected, dried with sodium sulfate, and concentrated for the determination of the intermediates using a Hewlett Packard 6890N GC/MSD. The extent of 4-CP mineralization was determined using the Total Organic Carbon, Method 10129 DR/4000 (HACH).

In order to evaluate the possibility of TPA leaching during the photocatalytic degradation of 4-CP, at the end of each experiment, the catalyst was separated by decantation, and W was determined in the liquid phase by atomic absorption spectrometry using a Varian AA Model 240 spectrophotometer. The calibration curve method was used, with standards prepared in the laboratory. The analyses were carried out at a wavelength of 254.9 nm, bandwidth 0.3 nm, lamp current 15 mA, phototube amplification 800 V, burner height 4 mm and acetylene–nitrous oxide flame (11:14).

The catalytic activity of the materials was compared with commercially available titania P25 Degussa measured in the same experimental conditions.

3. Results and discussion

The specific surface area (S_{BET}) of the modified titania was determined using the Brunauer–Emmett–Teller (BET) method, the specific surface area of micropores (S_{micro}) was estimated by the *t*-plot method, and the total pore volume and the average pore

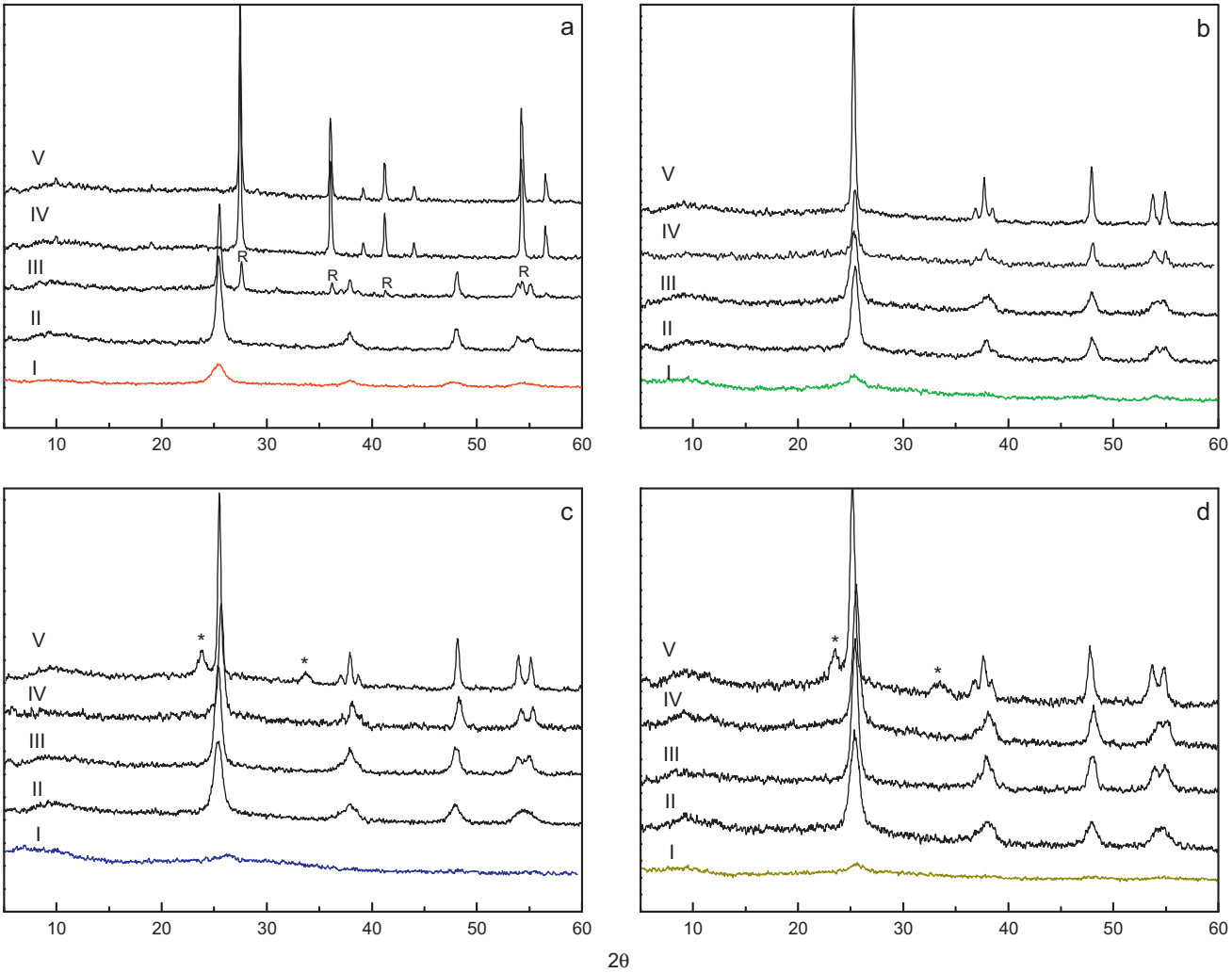

Fig. 1. XRD patterns of TiTPA00 (a), TiTPA10 (b), TiTPA20 (c), and TiTPA30 (d) samples, treated at 100 (I), 500 (II), 600 (III), 700 (IV), and 800 °C (V).

Table 1
Physicochemical properties of the TiTPA00 sample treated at different temperatures.

Sample	S_{BET} (m^2/g)	S_{micro}[a] (m^2/g)	D_p[b] (nm)	Total pore volume[c] (cm^3/g)	D_c[d] (nm)		E_g (eV)	pH_{PZC}[e]
					Anatase	Rutile		
$TiTPA00_{T100}$	372	35	3.1	0.195	5.9	–	3.20	6.5
$TiTPA00_{T500}$	56	–	6.1	0.184	13.3	–	3.10	5.9
$TiTPA00_{T600}$	21	–	13.1	0.088	20.9	6.1	2.99	5.7
$TiTPA00_{T700}$	5	–	13.9	0.016	–	22.3	3.00	5.6
$TiTPA00_{T800}$	3	–	14.2	0.007	–	23.4	2.99	5.6

[a] Specific surface area of micropores obtained from *t*-plot analysis.
[b] Average pore diameter calculated using the BJH formula from the desorption branch.
[c] Total pore volume calculated by the BJH method.
[d] Scherrer crystallite size estimated using the characteristic anatase (1 0 1) and rutile (1 1 0) diffraction planes.
[e] Ref. [33].

diameter (D_p) were obtained using the Barret–Joyner–Halenda (BJH) method. The results for the TiTPA00 sample calcined at different temperatures are shown in Table 1.

As can be observed, all the samples are mesoporous materials with a D_p higher than 3.1 nm. The specific surface area (S_{BET}) dramatically decreased and the mean pore radius increased when the calcination temperature was raised from 100 to 800 °C. According to the S_{micro} values, only the $TiTPA00_{T100}$ sample presents micropores, though less than 10% of the total specific surface area is due to a microporous structure.

The TPA-modified samples treated at 100 °C present lower S_{BET} values than the $TiTPA00_{T100}$ sample, and S_{BET} decreases in the following order: $TiTPA10_{T100}$ > $TiTPA20_{T100}$ > $TiTPA30_{T100}$ (Table 2), which may be due to a decrease in the cross-linking degree when the acid concentration increases. This result is in agreement with reports in the literature that indicates a similar behavior for the specific surface area of mesoporous titania obtained via a sol–gel process without the addition of any modifying compound [37,38].

The S_{BET} of TPA-modified samples also decreased when the calcination temperature was increased (Table 2), although the decrease of S_{BET} is lower for the samples with higher TPA content. This could be due to a strong interaction of the TPA incorporated into titania, which reduces the surface diffusion of titania, and inhibits sintering [39–41]. In addition, similar values of S_{BET} were found when 20% and 30% TPA was added, which would indicate a limiting value for the strong interaction mentioned above.

The XRD patterns of $TiTPA00_{T100}$, $TiTPA10_{T100}$, $TiTPA20_{T100}$, and $TiTPA30_{T100}$ samples (Fig. 1a) showed weak broad peaks in the same position where the characteristic peaks of the anatase phase are placed: 25.3° (1 0 1), 37.9° (0 0 4), 47.8° (2 0 0), and 54.3° 2θ. This is indicative of solids poorly crystallized and mostly amorphous. The crystallinity increased and the peak at 54.3° is split into two peaks at 54.0° and 54.9°, corresponding to the (1 0 5) and (2 1 1) reflections of the anatase phase, for the samples calcined at 500 °C.

The XRD pattern of the $TiTPA00_{T600}$ sample exhibited three new peaks at 2θ = 27.4°, 36.1°, and 54.2°, indicating that a partial transformation of anatase into rutile phase took place. The transformation was complete for the TiTPA00 sample treated at higher temperatures, because only the characteristic peaks of the rutile phase are present in the XRD pattern of $TiTPA00_{T700}$ and $TiTPA00_{T800}$.

On the other hand, the XRD patterns of TiTPA10, TiTPA20, and TiTPA30 samples calcined at 600, 700, and 800 °C (Fig. 1b, c, and d, respectively) showed only the presence of titania in an anatase-type structure, suggesting that the phase transition of anatase into rutile is shifted to higher temperatures in the presence of TPA. Additionally, the crystallinity increased when the calcination temperature was raised. However, the increment was lower for the samples with a higher TPA content.

The TiTPA20 and TiTPA30 samples calcined at 800 °C also display two new broad peaks at 2θ = 23.5° and 33.5°, which could be assigned to the presence of small crystals resulting from the thermal decomposition of TPA [42] that takes place at temperatures higher than 600 °C.

The results showed that the presence of TPA retarded the crystallization of titania and stabilized TiO_2 in the anatase phase, in agreement with literature reports of titania modified with tungsten oxide [40,43].

The crystallite size (D_C) of the samples, estimated from the XRD results using the Scherrer equation and silicon as standard for the correction of the instrumental broadening, are listed in Tables 1 and 2. As is generally reported, it was observed that D_C increases with the increment of the calcination temperature, the increase being lower for the samples with higher TPA content. This behavior may be attributed to crystal growth delay, which is very common in materials containing both a crystalline and an amorphous phase [44]. However, at each calcination temperature, the D_C values decrease in the following order TiTPA00 > TiTPA10 > TiTPA20 > TiTPA30 (Fig. 2).

The particle size distribution obtained from TEM for the $TiTPA00_{T100}$, $TiTPA10_{T100}$, $TiTPA20_{T100}$, and $TiTPA30_{T100}$ samples is shown in Fig. 3. As can be seen, the mean particle size (D_M) and the standard deviation (σ) increase with the increment of the TPA content. The particles displayed a size distribution between 5 and 45 nm.

These particles seem to be formed by the agglomeration of small primary particles (approximately 5 nm in size), as was reported by Carriazo et al. [45] for commercial titania samples impregnated with tungstophosphoric acid. The size of the agglomerates increased when both the TPA concentration in the solid and the

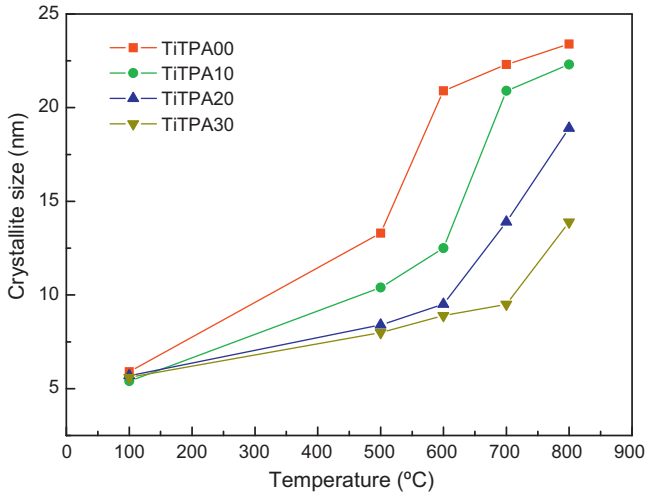

Fig. 2. Variation of D_C as a function of calcination temperature.

Table 2
Physicochemical properties of TPA-modified mesoporous titania treated at different temperatures.

Sample	S_{BET} (m^2/g)	D_p[a] (nm)	Total pore volume[b] (cm^3/g)	D_c[c] (nm) Anatase	E_g (eV)	pH_{PZC}[d]
$TiTPA10_{T100}$	296	3.4	0.208	5.4	3.05	6.2
$TiTPA20_{T100}$	276	3.6	0.175	5.7	3.02	6.0
$TiTPA30_{T100}$	247	3.9	0.143	5.6	2.99	5.5
$TiTPA10_{T500}$	78	5.2	0.180	10.4	2.95	5.3
$TiTPA20_{T500}$	106	4.1	0.150	8.4	2.90	4.6
$TiTPA30_{T500}$	116	4.2	0.159	8.0	2.88	2.8
$TiTPA10_{T600}$	58	8.2	0.157	12.5	2.95	5.2
$TiTPA20_{T600}$	69	5.8	0.135	9.5	2.89	4.6
$TiTPA30_{T600}$	93	5.4	0.155	8.9	2.87	2.9
$TiTPA10_{T700}$	34	10.4	0.109	20.9	2.94	5.2
$TiTPA20_{T700}$	46	8.9	0.104	13.7	2.89	4.6
$TiTPA30_{T700}$	75	6.4	0.151	9.5	2.86	2.8
$TiTPA10_{T800}$	20	12.7	0.072	22.3	2.94	5.1
$TiTPA20_{T800}$	31	12.6	0.077	18.9	2.88	4.5
$TiTPA30_{T800}$	44	9.3	0.131	13.9	2.84	2.8

[a] Average pore diameter calculated using the BJH formula from the desorption branch.
[b] Total pore volume calculated by the BJH method.
[c] Scherrer crystallite sizes estimated using the characteristic anatase (1 0 1) diffraction plane.
[d] Ref. [33].

thermal treatment temperature were higher, in the same way reported for titania samples modified with tungstosilicic acid [36].

According to the secondary electron micrographs, the samples consist of spherical particles, whose size increased from 200 to 800 nm when the TPA content was raised and remained practically unchanged during the calcination step. These spherical particles seem to be formed by aggregation of the nanoparticle agglomerates, as was reported by Bakardjieva et al. [46] for titania samples obtained by the hydrolysis of $TiOSO_4$ aqueous solution using urea as the precipitation agent. Additionally, the spherical particles are

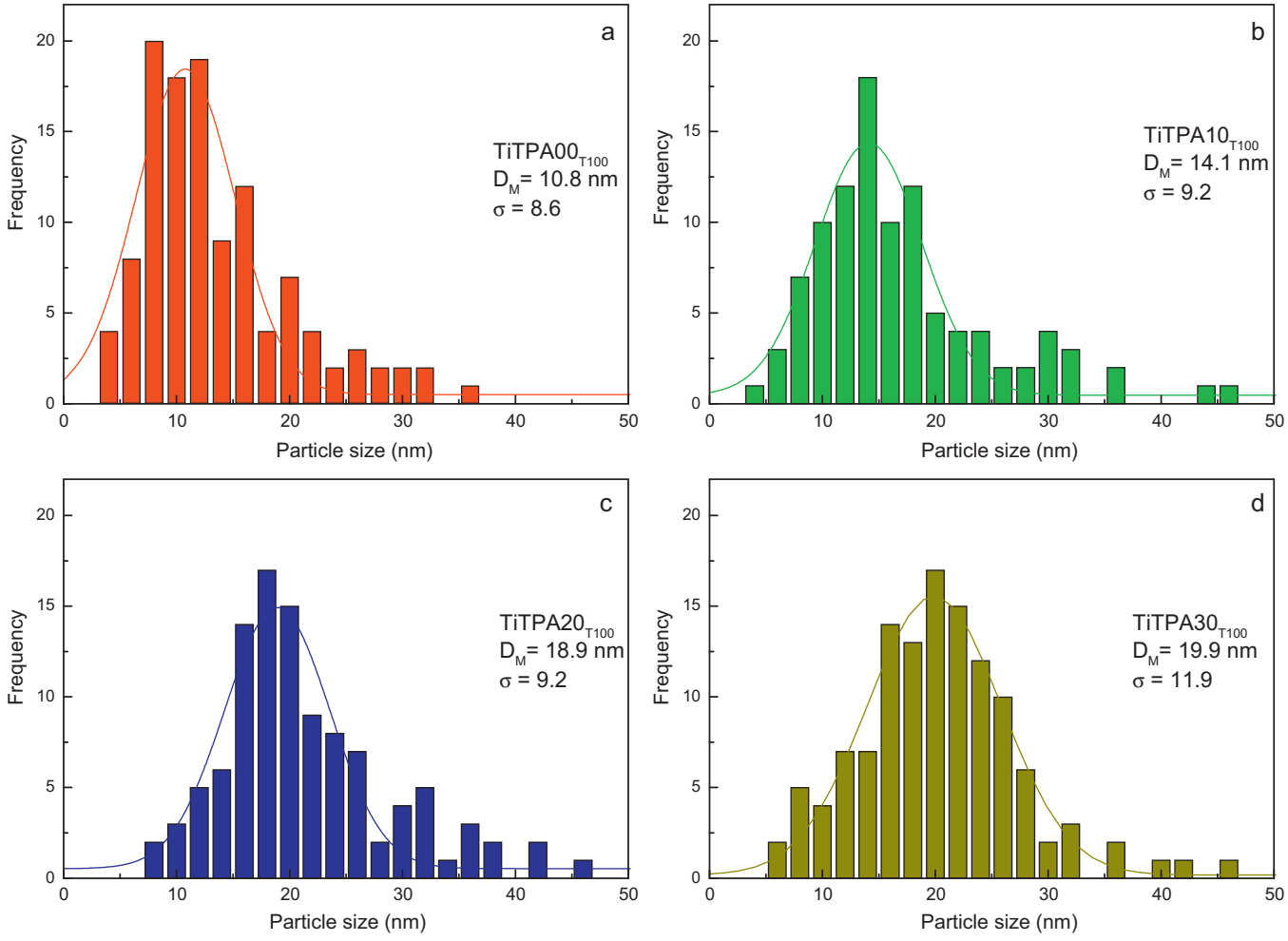

Fig. 3. Particle size distribution histograms based on TEM images of TiTPA00T100 (a), TiTPA10T100 (b), TiTPA20T100 (c), TiTPA30T100 and (d) samples.

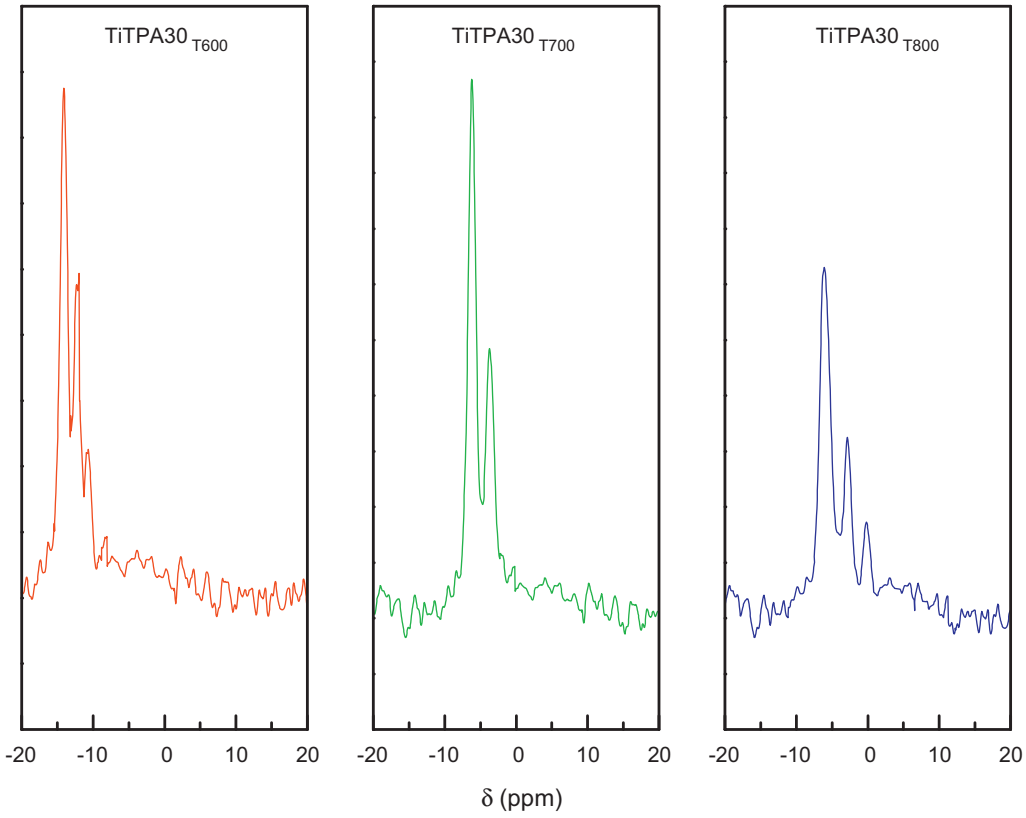

Fig. 4. 31P NMR spectra of TiTPA30T600, TiTPA30T700, and TiTPA30T800 samples.

present as clusters, whose size either slightly increased when the calcination temperature was raised (TiTPA00 and TiTPA10 samples) or remained practically unchanged (TiTPA20 and TiTPA30 samples).

From the FT-IR and ^{31}P MAS-NMR studies previously reported [33], we established that the main species present in the titania modified with TPA is the $[PW_{12}O_{40}]^{3-}$ anion that during the synthesis and subsequent thermal treatment up to 600 °C was partially transformed into the $[P_2W_{21}O_{71}]^{6-}$ and $[PW_{11}O_{39}]^{7-}$ species. The following transformation scheme $[PW_{12}O_{40}]^{3-} \Leftrightarrow [P_2W_{21}O_{71}]^{6-} \Leftrightarrow [PW_{11}O_{39}]^{7-}$ was proposed by Pope [47] when the pH is increased in solution. A similar change could partly take place in our samples as a result of localized pH increase during the synthesis.

The characteristic lines assigned to the presence of the $[PW_{12}O_{40}]^{3-}$, $[P_2W_{21}O_{71}]^{6-}$, and $[PW_{11}O_{39}]^{7-}$ anions at −14.5, −12.1, and −10.8 ppm, respectively, [48] are not present in the ^{31}P MAS-NMR spectra of TiTPA10, TiTPA20, and TiTPA30 samples calcined at 700 and 800 °C, as shown in Fig. 4 for the TiTPA30 sample.

The spectra of the samples treated at 700 °C display two wide lines with maximum at −6.2 and −3.0 ppm regarded as belonging to some species of unknown composition [49], as a result of the structure degradation of the $[PW_{12}O_{40}]^{3-}$, $[P_2W_{21}O_{71}]^{6-}$, and $[PW_{11}O_{39}]^{7-}$ anions during the calcination.

The spectra of $TiTPA10_{T800}$ and $TiTPA20_{T800}$ samples presented similar features to those calcined at 700 °C; however, the spectrum of the $TiTPA30_{T800}$ sample displays a new small line at 0.1 ppm assigned to phosphate species [50].

The UV–Vis-DRS spectra of TiTPA00 samples presented an intense absorption in the range 200–390 nm, corresponding to charge transfer from the valence band (O 2p) to the conduction band (Ti 3d) [51]. Bulk TPA displayed two absorption bands in the range 200–450 nm assigned to the charge transfer from bridging or terminal O 2p to W 5d (W–O–W and W–O_d, respectively) [24].

The UV–Vis-DRS spectra of TiTPA10, TiTPA20, and TiTPA30 samples displayed the shift of the charge transfer band to wavelength values closer to that of bulk TPA.

The band gap values (E_g) were estimated from the corresponding Kubelka–Munk remission functions, calculated from the absorbance values of the DRS spectra [52]. The band gap energy of TiTPA00 samples was in the range 3.20–2.99 eV (Table 1). The values decreased when the calcination temperature increased, probably as a result of a higher crystallinity and the appearance of the rutile phase [53]. The E_g values of the modified titania samples slightly decreased with the TPA content (Table 2), but they remained almost constant with the temperature increase.

The point of zero charge of the solids treated at 100 °C decreased in parallel with the increment of tungstophosphoric acid in the samples (Tables 1 and 2). The pH_{PZC} diminished when the calcination temperature was raised from 100 to 500 °C and remained almost constant for higher temperatures.

The prepared materials were tested in the photocatalytic degradation of 4-chlorophenol (4-CP) at the pH of the suspension obtained by the addition of 100 mg of catalyst to 200 ml of a 4-CP water solution (1.5×10^{-4} mol/l). The initial and the final pH of the solutions were in the range 7.0–5.5. The 4-CP (a weak acid of $pKa = 9.41$) under this experimental condition was mainly present in the non ionized form, and the surface of the catalysts was mostly negatively charged. As a result, an important adsorption of 4-CP on the catalyst surface does not take place.

The variation of 4-CP concentration as a function of time using the $TiTPA00_{T100}$, $TiTPA10_{T100}$, $TiTPA20_{T100}$, and $TiTPA30_{T100}$ samples is shown in Fig. 5a. The reduction in the 4-CP concentration was lower than 9% for the $TiTPA00_{T100}$ sample at 240 min under reaction. However, for the TPA-modified samples, the 4-CP degradation at the same time is significantly higher, and the 4-CP concentration decline increases in parallel with the

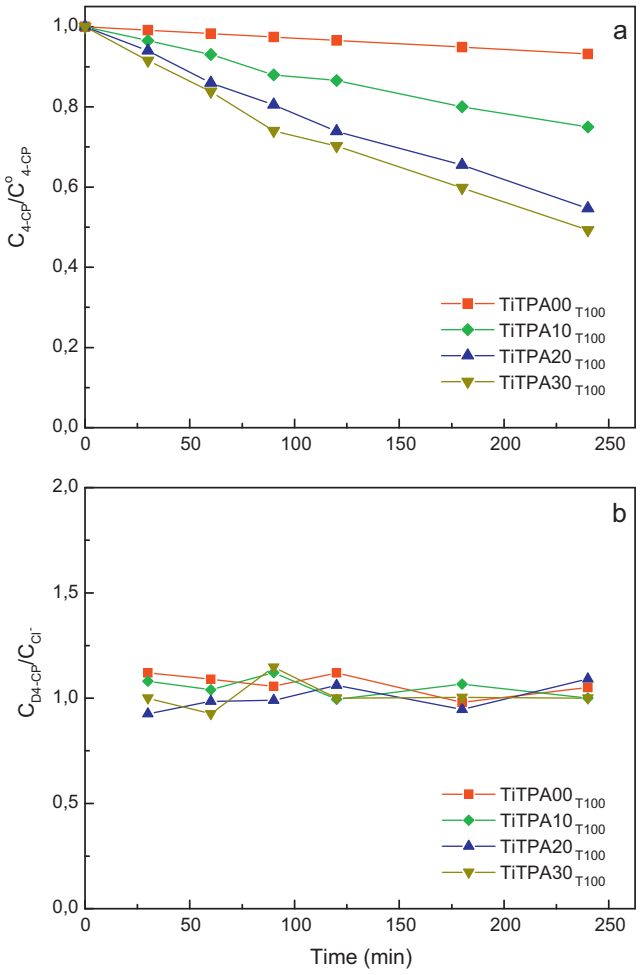

Fig. 5. Photocatalytic degradation of 4-CP (a) and ratio between the amount of degraded 4-CP and the amount of released chloride ions as a function of the irradiation time (b) for the TiTPA samples treated at 100 °C.

increment of tungstophosphoric acid in the samples: $TiTPA10_{T100}$ (25%) < $TiTPA20_{T100}$ (45%) < $TiTPA30_{T100}$ (51%).

The amount of 4-CP degraded after 240 min of irradiation but without catalyst was only of 6%, and it is mainly due to a photolytic process [54]. 4-CP degradation was not detected under the same experimental conditions but with the mercury lamp turned off.

The ratio between the amount of degraded 4-CP (C_{D4C-P}) and the amount of released chloride ions (C_{Cl^-}) as a function of the irradiation time is shown in Fig 5b. As can be observed, both amounts remain basically equal during the course of the photodegradation. These results are in agreement with previous reports that indicate that the cleavage of the Cl-aryl bond, releasing inorganic chloride to the reacting medium, is the first step during the photocatalytic degradation of 4-CP. Many studies have reported the appearance of benzoquinone (BQ), hydroquinone (HQ) and 4-chlorocatechol (4-CC) as the predominant aromatic reaction intermediates during the photodegradation of 4-CP [55–57]. However, their nature and amount depend on the catalyst and the experimental conditions.

Mylonas and Papaconstantinou [25] and Yue et al. [58] found that hydroquinone and benzoquinone were the major intermediaries when 4-CP was photodegraded using polyoxometallates and silica-immobilized polyoxometallates, respectively.

According to Kormali et al. [59], some of the intermediates detected during the 4-CP photodegradation catalyzed by $[PW_{12}O_{40}]^{3-}$ were not found or were present as traces (HQ and 4-CC respectively) when TiO_2 was used. They suggest that this fact is due to the photodegradation catalyzed by $[PW_{12}O_{40}]^{3-}$ essentially operates via •OH radicals, while holes and •OH radicals take part in the case of TiO_2 photocatalysis. In our experimental conditions, we found that BQ was the predominant intermediate and only traces of HQ and 4-CC were detected.

The 4-CP degradation profiles using TiTPA00, TiTPA10, TiTPA20, and TiTPA30 samples annealed at temperatures higher than 100 °C are shown in Fig. 6. The data indicate that for the TiTPA00 and TPA-modified samples, the 4-CP degradation rates increased when the calcination temperature was raised up to 500 and 600 °C respectively, and decreased at higher temperature values. Additionally, when a particular temperature is considered, the amount of degraded 4-CP increased with the increment of the TPA content. On the other hand, all the samples presented higher degradation rates than those treated at 100 °C.

The degradation profiles of 4-CP using TiO_2 Degussa P25 (Fig. 6), shown as reference, are very similar to those of the $TiTPA00_{500}$ and $TiTPA10_{500}$ samples.

The photocatalytic degradation of 4-CP in aqueous systems can be described by a pseudo-first-order kinetics with respect to the dye concentration [60–62], which results from considering that the reaction rate follows the Langmuir–Hinshelwood model

$$r_{4\text{-CP}} = -\frac{dC_{4\text{-CP}}}{dt} = \frac{k_r K C_{4\text{-CP}}}{1 + K C_{4\text{-CP}}}$$

where $r_{4\text{-CP}}$ is the degradation rate, $C_{4\text{-CP}}$ is the 4-CP concentration, and k_r and K are the reaction and the adsorption constants, respectively. When $C_{4\text{-CP}}$ is low, $KC_{4\text{-CP}}$ is generally negligible and the reaction rate can be assumed as of pseudo-first-order with respect to the dye concentration. The resultant equation can be integrated considering that $C_{4\text{-CP0}}$ is the 4-CP concentration at time equal zero, so

$$\ln\left(\frac{C_{4CP0}}{C_{4\text{-CP}}}\right) = k_r K\, t$$

From the plots of $\ln(C_{4\text{-CP0}}/C_{4\text{-CP}})$ as a function of time, the values of the apparent reaction constant $k_{ap} = k_r \times K$ were obtained, and are shown in Fig. 7.

The k_{ap} values of the TiTPA00 sample increased when the calcination temperature was raised up to 500 °C, and then decreased continuously when the sample was calcined at higher temperatures (Fig. 7). The increase of k_{ap} is attributed to the higher crystallinity of the $TiTPA00_{T500}$ sample compared with that treated at 100 °C, and is slightly lower than the value estimated for TiO_2 Degussa P25 ($k_{ap} = 1.05 \times 10^{-2}\ min^{-1}$).

As a result of the higher crystallinity, the number of defects, which act as recombination centers for the photogenerated electrons and holes, decreased and k_{ap} increased [63–66]. The transformation of anatase into rutile phase and the drop of S_{BET} are ascribed to be responsible for the decrease of k_{ap} observed for the samples calcined at higher temperatures [67].

The k_{ap} values of the samples annealed at 100 °C slightly increase in the following order: $TiTPA00_{T100}$ < $TiTPA10_{T100}$ < $TiTPA20_{T100}$ < $TiTPA30_{T100}$, showing the positive effect of the modification with TPA in the catalytic activity of titania. Taking into account that all the samples are poorly crystallized solids and that the S_{BET} values decreases in the reverse order, the increase of k_{ap} values with the TPA content may be considered as indicative of the participation of TPA in the decrease of the recombination degree of photogenerated charges, as was suggested by Park and Choi [31]. A similar explanation was proposed by Fuerte et al. [68] to explain the continuous enhancement of the photocatalytic activity in the degradation of toluene when increasing the percentage of W present in the anatase structure of TiO_2 doped with ammonium tungstate solutions.

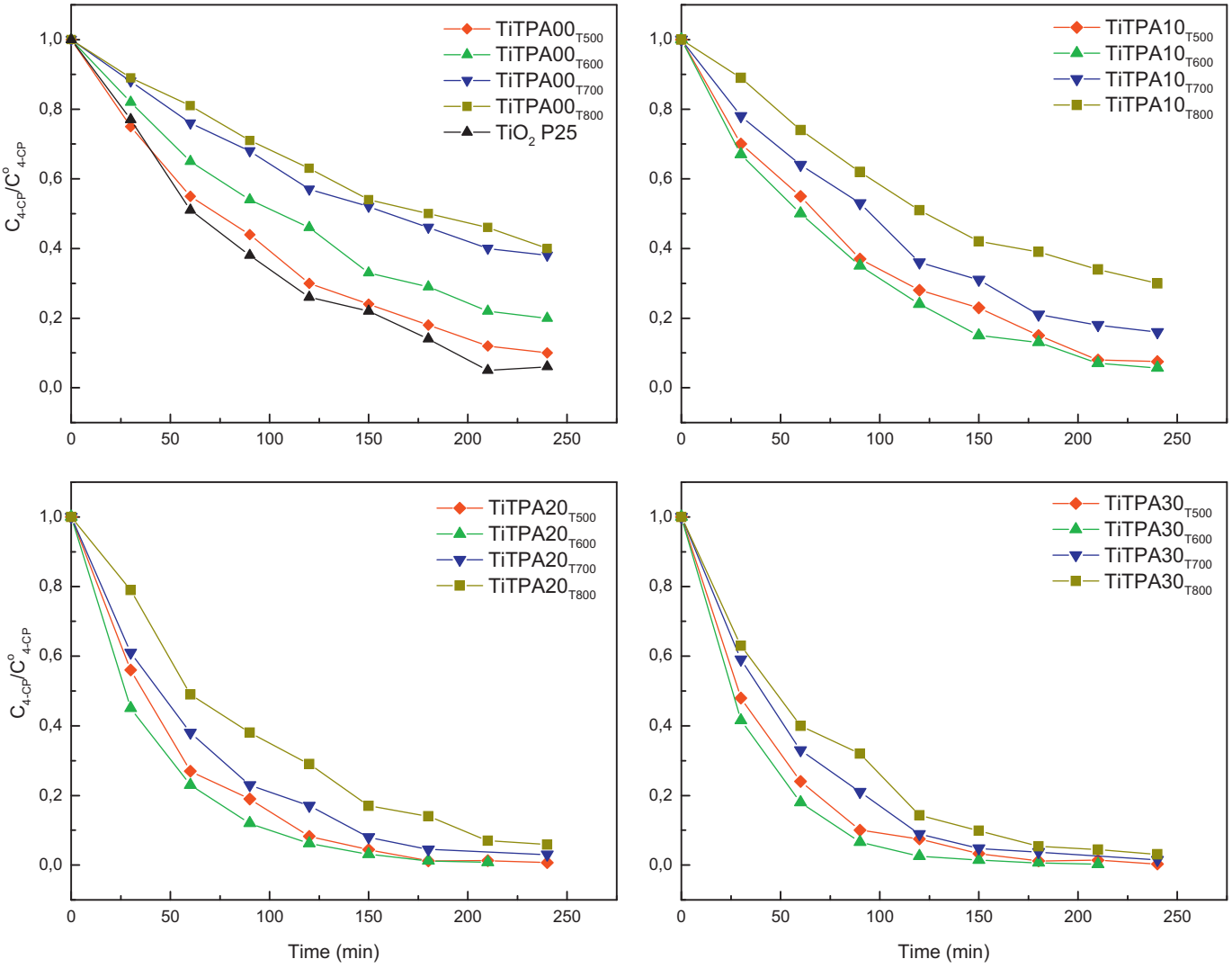

Fig. 6. Photocatalytic degradation of 4-CP as a function of the irradiation time for the TiTPA samples treated at 500, 600, 700, 800 °C, and TiO2 Degussa P25.

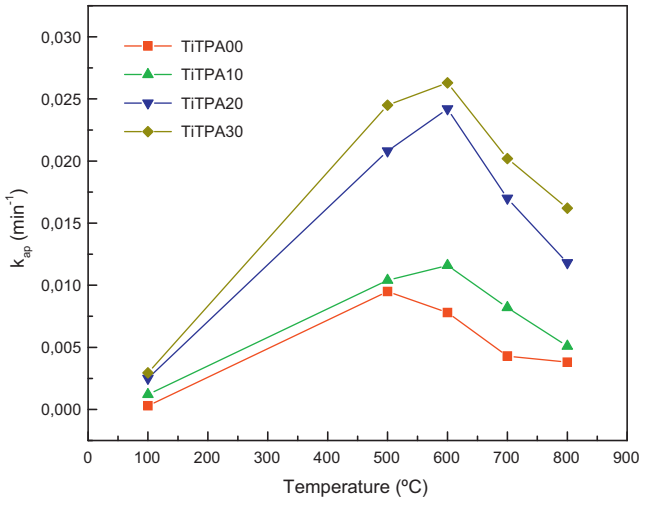

Fig. 7. Apparent reaction constant *k*ap of the 4-CP photocatalytic degradation as a function of the thermal treatment temperature.

Additionally, the increment of the catalytic activity could be due to the direct participation of TPA in the degradation of the organic substrate (reactions (1)–(3)) and/or in the production of •OH reactive species (reaction (6)) that participates in the degradation of the organic substrate (reaction (7)) [69].

$$POM^{*} + H_2O \rightarrow POM^{-} + {}^{\bullet}OH + H^{+} \quad (6)$$

$${}^{\bullet}OH + S \rightarrow \text{oxidationproducts} \quad (7)$$

Regardless the thermal treatment temperature employed, k_{ap} values of the TPA-modified samples are higher than those of TiTPA00. They increased with the rise of TPA content, though the increase is small for TiTPA10 samples. Additionally, the k_{ap} values also increased with the increment of the calcination temperature from 100 up to 600 °C and then decreased. The diminution in k_{ap} could be assigned to both the S_{BET} drop and the structure disruption of the $[PW_{12}O_{40}]^{3-}$, $[P_2W_{21}O_{71}]^{6-}$, and $[PW_{11}O_{39}]^{7-}$ anions during the thermal treatment, as was revealed by ^{31}P MAS-NMR.

Regardless the TPA content, all the TPA-modified samples calcined at 500 and 600 °C present the highest k_{ap} values, which are also higher than that of TiO_2 Degussa P25.

In sum, the addition of TPA to titania prepared by the sol–gel type reaction, using urea as a low-cost pore-forming agent, led to

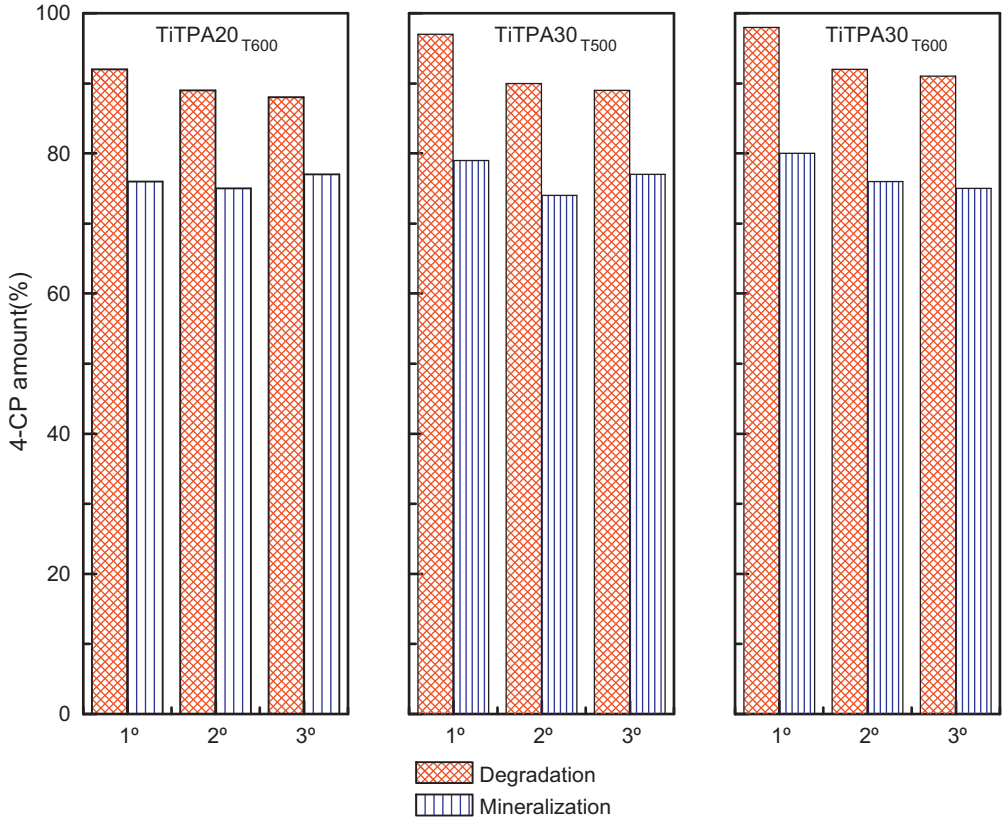

Fig. 8. 4-CP degradation and mineralization degree as a function of the number cycle of usage for the TiTPA20T600, TiTPA30T500, and TiTPA30T600 catalysts.

materials with a good behavior as catalysts for 4-CP photodegradation. It is clearly observed that the reaction rate was affected not only by the TPA amount but also by the thermal treatment, and that different factors are involved in the catalytic performance. Taking into account the obtained results, the highest activity with the lowest preparation cost resulted from the catalyst prepared by adding 30% TPA calcined at 600 °C.

Nevertheless, the three samples that showed better catalytic performance ($TiTPA20_{T600}$, $TiTPA30_{T500}$, and $TiTPA30_{T600}$) were chosen to test their reusability, because they have a similar apparent reaction constant. To this end, after each photocatalytic experiment, the catalysts were easily separated from the resulting suspension by decantation, washed with distilled water, dried at 70 °C and reused.

The percentage of degraded 4-CP after each cycle of usage, together with the mineralization degree, is shown in Fig. 8. The mineralization degree was slightly lower than the amount of degraded 4-CP as a result of the formation of organic intermediates previously mentioned. The results indicated that both remain practically unchanged for the $TiTPA20_{T600}$ sample. In the case of the $TiTPA30_{T500}$ and $TiTPA30_{T600}$ samples, both the percentage of 4-CP degraded and the mineralization degree decrease slightly during the first reuse, and then keep constant. The decrease was assigned to the solubilization of TPA (less than 1% of the TPA content) from the fresh samples during the first catalytic test, as was established by atomic absorption spectrometry. On the other hand, these results show that after the third use the catalytic performance of the selected samples is the same. So, adequate reusable photocatalysts to degrade a toxic chlorinated phenol have been developed.

4. Conclusions

Mesoporous titania directly modified with TPA was synthesized by sol–gel type reactions using urea as a pore-forming agent, obtaining solids with an average pore diameter higher than 3.1 nm and the anatase structure of titania. The specific surface area decreased when both the TPA amount and the calcination temperature increased.

The crystallite size increased with the calcination temperature, but lower values were obtained for higher TPA content. The Keggin structure of the tungstophosphate anion is partially transformed when the samples are thermally treated up to 600 °C and, at higher temperature, the structure is degraded.

The direct modification of titania with TPA is a good method to obtain catalysts with higher photocatalytic activity in the 4-chlorophenol degradation. The apparent reaction constant, estimated assuming a pseudo-first-order kinetics, showed that the catalyst behavior depended on the TPA amount and the thermal treatment temperature, the solid containing 30% TPA calcined at 600 °C being more effective. In addition, the reused catalysts showed only a slight decrease in the degradation and mineralization degree, thus being promissory materials to aid in the photocatalytic treatment of wastewater that contain chlorinated phenols.

Acknowledgements

The authors thank E. Soto, L. Osiglio, G. Valle, and L. Méndez for their experimental help, and the financial support of CONICET and UNLP.

References

[1] Y. Pi, L. Zhang, J. Wang, J. Hazard. Mater. 141 (2007) 707–712.
[2] D. Chen, A.K. Ray, Appl. Catal. B: Environ. 23 (1999) 143.
[3] J. Theurich, M. Lindner, D.W. Bahnemann, Langmuir 12 (1996) 6368.
[4] M.A. Fox, M.T. Dulay, Chem. Rev. 93 (1993) 341.
[5] S. Anandan, A. Vinu, N. Venkatachalam, B. Arabindoo, V. Murugesan, J. Mol. Catal. A: Chem. 256 (2006) 312.
[6] M.R. Hoffman, S.T. Martin, W. Choi, D.W. Bahnemann, Chem. Rev. 95 (1995) 69.
[7] A.D. Paola, E. Garcia-Lopez, S. Ikeda, G. Marci, B. Ohtani, L. Palmisano, Catal. Today 78 (2002) 87–93.
[8] X. Li, J.W. Cubbage, T.A. Tetzlaff, W.S. Jenks, J. Org. Chem. 64 (1999) 8509–8524.
[9] A. Sclafani, L. Palmisano, M. Schiavello, J. Phys. Chem. 94 (1990) 829.
[10] K.B. Kyoko, S. Kazuhiro, K. Hitoshi, O. Kiyomi, A. Hironori, Appl. Catal. A: Gen. 165 (1997) 394.
[11] S. Sakulkhaemaruethai, S. Pavasupree, Y. Suzuki, S. Yoshikawa, Mater. Lett. 59 (2005) 2965.
[12] J.-Y. Zheng, J.-B. Pang, K.-Y. Qiu, Y. Wei, Micropor. Mesopor. Mater. 49 (2001) 189.
[13] L.R. Pizzio, Mater. Lett. 59 (2005) 994.
[14] W. Lee, Y.M. Gao, K. Dwight, A. Wold, Mater. Res. Bull. 27 (1992) 685.
[15] A. Sclafani, M.N. Mozzanega, P.J. Pichat, Photochem. Photobiol. A: Chem. 59 (1991) 181.
[16] W. Lee, Y.R. Do, K. Dwight, A. Wold, Mater. Res. Bull. 28 (1993) 1127.
[17] S. Ikeda, N. Sugiyama, B. Pal, G. Marci, L. Palmisano, H. Noguchi, K. Uosaki, B. Ohtani, Phys. Chem. Chem. Phys. 3 (2001) 267.
[18] M. Anpo, Catal. Surv. Jpn. 1 (1997) 169.
[19] Y.R. Do, W. Lee, K. Dwght, A. World, J. Solid State Chem. 108 (1994) 198.
[20] K. Tennakone, O.A. Haperuna, J.M. Bandara, W.C.B. Kiridena, Semicond. Sci. Technol. 7 (1992) 423.
[21] G. Marci, L. Palmisano, A. Sclafani, A.M. Venezia, R. Campostrini, G. Carturan, C. Martín, V. Rives, G. Solana, J. Chem. Soc., Faraday Trans. 92 (1996) 819.
[22] T. Okuhara, N. Mizuno, M. Misono, Adv. Catal. 41 (1996) 221.
[23] V.M. Fuchs, L.R. Pizzio, M.N. Blanco, Catal. Today 133–135 (2008) 181.
[24] L.R. Pizzio, C.V. Cáceres, M.N. Blanco, Appl. Catal. A: Gen. 167 (1998) 283.
[25] A. Mylonas, E. Papaconstantinou, J. Photochem. Photobiol. 94 (1996) 77.
[26] C. Hu, B. Yue, T. Yamase, Appl. Catal. A: Gen. 194–195 (2000) 99.
[27] R.R. Ozer, J.L. Ferry, J. Phys. Chem. B 104 (2000) 9444.
[28] R.R. Ozer, J.L. Ferry, Environ. Sci. Technol. 35 (2001) 3242.
[29] M. Yoon, J.A. Chang, Y. Kim, J.R. Choi, K. Kim, S.J. Lee, J. Phys. Chem. B 105 (2001) 2539.
[30] Y. Yang, Y. Guo, C. Hu, Y. Wang, E. Wang, Appl. Catal. A: Gen. 273 (2004) 201.
[31] H. Park, W. Choi, J. Phys. Chem. B 107 (2003) 3885.
[32] L. Li, Q.-Y. Wu, Y.-H. Guo, Ch.-W. Hu, Micropor. Mesopor. Mater. 87 (2005) 1.
[33] V.M. Fuchs, E.L. Soto, M.N. Blanco, L.R. Pizzio, J. Colloid Interface Sci. 327 (2008) 403.
[34] M.N. Blanco, L.R. Pizzio, Appl. Surf. Sci. 256 (2010) 3546.
[35] V.M. Fuchs, L. Méndez, M.N. Blanco, L.R. Pizzio, Appl. Catal. A: Gen. 358 (2009) 73.
[36] M.N. Blanco, L.R. Pizzio, Handbook of Photocatalysts: Preparation, Structure and Applications, Nova Science Publishers, Hauppauge NY, 2009, pp. 511–526.
[37] N. Phonthammachai, T. Chairassameewong, E. Gulari, A.M. Jamieson, S. Wongkasemjit, Micropor. Mesopor. Mater. 66 (2003) 261.
[38] K.M.S. Khalil, T. Baird, M.I. Zaki, A.A. El-Samahy, A.M. Awad, Colloid Surf. A 132 (1998) 31.
[39] S. Eibil, B.C. Gates, H. Knozinger, Langmuir 17 (2001) 107.
[40] X.-F. Yu, N.-Z. Wu, H.-Z. Huang, Y.-C. Xie, Y.-Q. Tang, J. Mater. Chem. 11 (2001) 3337.
[41] S.M. Kumbar, G.V. Shanbhag, F. Lefebvre, S.B. Halligudi, J. Mol. Catal. A: Chem. 256 (2006) 125.
[42] J.B. Mioc, R.Z. Dimitrijevi, M. Davidovic, Z.P. Nedic, M.M. Mitrovic, P.H. Colomban, J. Mater. Sci. 29 (1994) 3705.
[43] H. Yang, D. Zhang, L. Wang, Mater. Lett. 57 (2002) 674.
[44] E. Ortiz-Islas, T. López, R. Gómez, M. Picquart, D.H. Aguilar, P. Quintana, Appl. Surf. Sci. 252 (2005) 853.
[45] D. Carriazo, M. Addamo, G. Marcì, C. Martín, L. Palmisano, V. Rives, Appl. Catal. A: Gen. 356 (2009) 172.
[46] S. Bakardjieva, J. Šubrt, V. Štengl, V. Balek, M.J. Dianez, M.J. Sayagues, Appl. Catal. B: Environ. 58 (2005) 193.
[47] T. Pope, Heteropoly and Isopoly Oxometalates, Springer-Verlag, Heidelberg, 1983, p. 58.
[48] R. Massart, R. Contant, J. Fruchart, J. Ciabrini, M. Fournier, Inorg. Chem. 16 (1977) 2916.
[49] L.R. Pizzio, C.V. Cáceres, M.N. Blanco, Appl. Surf. Sci. 151 (1999) 91.
[50] J.A.R. van Veen, O. Sudmeijer, C.A. Emeis, H. de Wit, J. Chem. Soc., Dalton Trans. (1986) 1825.
[51] R.D. Shannon, Acta Crystallogr. A 32 (1976) 751.
[52] E. Joselevich, I. Willner, J. Phys. Chem. 98 (1994) 7628.
[53] S.P. Tandom, J.P. Gupta, Phys. State Solids 38 (1970) 363.
[54] M.A. Barakat, H. Schaeffer, G. Hayes, S. Ismat-Shah, Appl. Catal. B: Environ. 57 (2005) 23.
[55] M.G. Kang, H.E. Han, K.J. Kim, J. Photochem. Photobiol. A: Chem. 125 (1999) 119.
[56] H.H. Oua, S.L. Loa, C.H. Wu, J. Hazard. Mater. B 137 (2006) 1362.
[57] N. Venkatachalam, M. Palanichamy, B. Arabindoo, V. Murugesan, J. Mol. Catal. A: Chem. 266 (2007) 158.
[58] B. Yue, Y. Zhou, J. Yuxu, Z. Wu, X. Zhang, Y. Zou, S. Jin, Environ. Sci. Technol. 36 (2002) 1325.
[59] P. Kormali, A. Troupis, T. Triantis, A. Hiskia, E. Papaconstatinou, Catal. Today 124 (2007) 149.
[60] C. Lettmann, K. Hindenbrand, H. Kisch, W. Macyk, W.F. Maier, Appl. Catal. B: Environ. 32 (2001) 215.
[61] G. Sivalingam, M.H. Priya, G. Madras, Appl. Catal. B: Environ. 51 (2004) 67.
[62] Y. Cheng, H. Sun, W. Jin, N. Xu, Chem. Eng. J. 128 (2007) 127.
[63] K.J. Jung, S.B. Park, Appl. Catal. B: Environ. 25 (2000) 249.
[64] H. Kominami, J. Kato, S. Murakami, Y. Ishii, M. Kohno, K. Yabutani, T. Yamamoto, Y. Kera, M. Inoue, T. Inui, B. Ohtani, Catal. Today 84 (2003) 181.
[65] J.G. Yu, H.G. Yu, B. Cheng, X.J. Zhao, J.C. Yu, W.K. Ho, J. Phys. Chem. B 107 (2003) 13871.
[66] C. Guillard, J. Disdier, J.M. Herrmann, C. Lehaut, T. Chopin, S. Malato, J. Blanco, Catal. Today 54 (1999) 217.
[67] C. Su, B.-Y. Hong, C.-M. Tseng, Catal. Today 96 (2004) 119.
[68] A. Fuerte, M.D. Hernández-Alonso, A.J. Maira, A. Martínez-Arias, M. Fernández-García, J.C. Conesa, J. Soria, G. Munuera, J. Catal. 212 (2002) 1.
[69] S. Antonaraki, T.M. Triantis, E. Papaconstantinou, A. Hiskia, Catal. Today 151 (2010) 119.